

# Synthesis of Co(II), Ni(II), Cu(II), Pd(II), and Pt(IV) Complexes with 1<sup>4</sup>,1<sup>5</sup>,3<sup>4</sup>,3<sup>5</sup>-Tetrahydro-1<sup>1</sup>H, 3<sup>1</sup>H-4,8-diaza-1,3(3,4)-diazola-2,6(1,4)-dibenzenacyclooctaphane-4,7-dien-1<sup>5</sup>,3<sup>5</sup>-dithione, and the Thermal Stability of Polyvinyl Chloride Modified Complexes

Ali Mudher Abdulkareem Al-Khazraji\*

Department of Chemistry, College of Education for Pure Science Ibn Al-Haitham, University of Baghdad, Baghdad, Iraq

\* **Corresponding author:**

tel: +964-7724031983

email:

ali.m.ak@ihcoedu.uobaghdad.edu.iq

Received: January 13, 2023

Accepted: February 16, 2023

DOI: 10.22146/ijc.81272

**Abstract:** In the current endeavor, a new Schiff base of 1<sup>4</sup>,1<sup>5</sup>,3<sup>4</sup>,3<sup>5</sup>-tetrahydro-1<sup>1</sup>H,3<sup>1</sup>H-4,8-diaza-1,3(3,4)-diazola-2,6(1,4)-dibenzenacyclooctaphane-4,7-dien-1<sup>5</sup>,3<sup>5</sup>-dithione was synthesized. The new symmetrical Schiff base (Q) was employed as a ligand to produce new complexes comprising Co(II), Ni(II), Cu(II), Pd(II), and Pt(II) metal-ions at a ratio of 2:1 (Metal:ligand). There have been new ligands and their complexes validated by (FTIR), (UV-visible), <sup>1</sup>H-NMR, <sup>13</sup>C-NMR, CHNS, and FAA spectroscopy, Thermogravimetric analysis (TG), Molar conductivity, and Magnetic susceptibility. The photostabilization technique to enhance the polymer was also used. The ligand Q and its complexes were mixed in 0.5% w/w of polyvinyl chloride in tetrahydrofuran (THF). The photo stabilization of polymer films was studied at 25 °C under irradiation of light λ 380–250 nm with intensity of 7.75 × 10<sup>-9</sup> ein dm<sup>-3</sup> s<sup>-1</sup>. The photostabilization activity of these compounds was determined by monitoring the hydroxyl, carbonyl, and polyene indexes, weight loss method with irradiation time. The I<sub>CO</sub>, I<sub>PO</sub> and I<sub>OH</sub> index values increased with irradiation time, this increase depends on the type of additives. The surface morphology for these films was studied during irradiation time. This project is highly intriguing for the ecosystem in regards to the decrease in the consumption of plastic.

**Keywords:** Schiff base; PVC; photostability; photodegradation; PVC films; weight loss

## ■ INTRODUCTION

Chemical compounds with at least two diversified atom types in the rings are known as hetero cycles [1]. Organic hetero cyclic encompass ringed blended rings without atoms and heteroatoms (N, O, and S). Most organic compounds have at least one heterocyclic sequence to make them the most predominant variety of compounds; hetero-atom presence provides heterocyclic compounds with numerous physical and chemical characteristics. Heterocycles are found in many organic ingredients such as vitamins, hormones [2], antibiotics [3], and pigments [4], and each of the main constituents are critical to human health. Therefore, we can conclude that the concept of biologically active molecules is becoming more widely discussed. Biologically active natural products are impeded by heterocyclic nitrogen, a synthetic compound. Chemically, triazole is part of the class of organic heterocyclic compounds called pyridazines [5]. It has two

carbon atoms at the non-adjacent site and belongs to a class of five unsaturated ring structure members with three atoms each; the isomer resembles the triazole.

The triazole ring is a planar geometry that possesses a resonance system through (6 π-electron) delocalized for carbon atoms and π-electron distortion system due to nitrogen atoms for both types (symmetrical and vicinal formula). Through the phenomenon of resonance in the five-ring system represented by the triazole ring, it adds to its high stability through the exchange of electrons and is known as tautomerism state by conjugate bonds with an π-electron with nitrogen atoms. In two unique tautomeric forms, 1,2,4-triazoles [6] are feasible; pharmaceutically, the 1,2,4-triazole-1H and 4-hydro-1,2,4-triazole is considered essential.

In sequence, for the amine and sulfur atom to take effect, soft, and hard nitrogen atoms must constitute an

exquisite ligand. This new Schiff base ligand interacts with the terephthaldehyde [7].

Additionally, considerable investigation into the coordination of divalent metal ions can be conducted using this newer Schiff base [8]. Metal transition complexes are the ongoing inspiration for us in our experiments. The polyvinyl chloride film [9] is judged for photodegradation to accurately assess newer compounds in a photostability operation to synthesize, characterize, and test the new ligand (Schiff base) and complexes. When it comes to nitrogen, neither soft nor hard instances must be attached to the same ligand. Terephthaldehyde and the new Schiff base [10] ligand, interact with each other. The coordination of various metal ions is also used to study the functioning of this novel Schiff base and its procedures. Metal transition complexes are an ongoing attraction for us in our research. The polyvinyl chloride film is judged for photodegradation to judge new compounds in a photostability [11] set-up to synthesize, characterize, and test the new ligand (Schiff base) and complexes through monitoring the degree of polymerization, weight loss, hydroxyl, carbonyl, and polyene index.

## ■ EXPERIMENTAL SECTION

### Materials

All the chemicals used in this research were supplied by Sigma-Aldrich without any additional purification. Terephthalic acid, absolute EtOH, Carbon-disulfide  $\text{CS}_2$ , Hydrazine hydrate 80%, Glacial acetic acid, Sulfuric acid, Potassium hydroxide KOH, Sodium bicarbonate  $\text{NaHCO}_3$ , Diethyl ether, the metal salt  $\text{CoCl}_2 \cdot 6\text{H}_2\text{O}$ ,  $\text{CuCl}_2 \cdot 2\text{H}_2\text{O}$ ,  $\text{NiCl}_2 \cdot 6\text{H}_2\text{O}$ ,  $\text{PdCl}_2 \cdot 2\text{H}_2\text{O}$ , and  $\text{PtCl}_6 \cdot 6\text{H}_2\text{O}$  and Polyvinyl chloride  $(\text{CH}_2\text{CHCl})_n$  were all obtained from Sigma-Aldrich.

### Instrumentation

The instrumentations used in this study were The Fourier transform Infrared (FTIR) spectra ( $400\text{--}4000\text{ cm}^{-1}$ ) recorded on a Shimadzu 8400 Spectrophotometer (Shimadzu Cooperation, Kyoto, Japan) using the KBr disc technique. Proton nuclear spectrum for Schiff base (Q) magnetic resonance ( $^1\text{H-NMR}$ ,  $^{13}\text{C-NMR}$ ) spectra

( $400\text{ MHz}$ ,  $125\text{ MHz}$ ) recorded on a Bruker DRX400 NMR Spectrometer (Bruker, Zürich, Switzerland) in  $\text{DMSO-}d_6$  related to tetramethylsilane. Conductivity measurements were conducted with the WTW, USA. The chloride content was measured with the 686-Titro Processor-665 Dosim A-Metrohm/Swiss. Magnetic susceptibility measurements were conducted with the Bruker BM6 instrument. The electronic spectra used A Shimadzu-160 spectrophotometer ( $200\text{--}900\text{ nm}$ ; Kyoto, Japan). The atomic absorption (A.A.) technique was performed using a Shimadzu PR-5 ORAPHIC PRINTER atomic absorption spectrophotometer. The melting point was determined by the Gallen Kamp Apparatus. The elemental analyses were performed on the Vario EL III Elementar instrument. A Digital Caliper,  $1000\text{ mm}/40\text{-inch}$  Vogel, Germany was utilized to prepare PVC films. The morphology images of PVC films were recorded on the Meiji Techno Microscope (Meiji Techno, Tokyo, Japan), ( $460\times$  magnification).

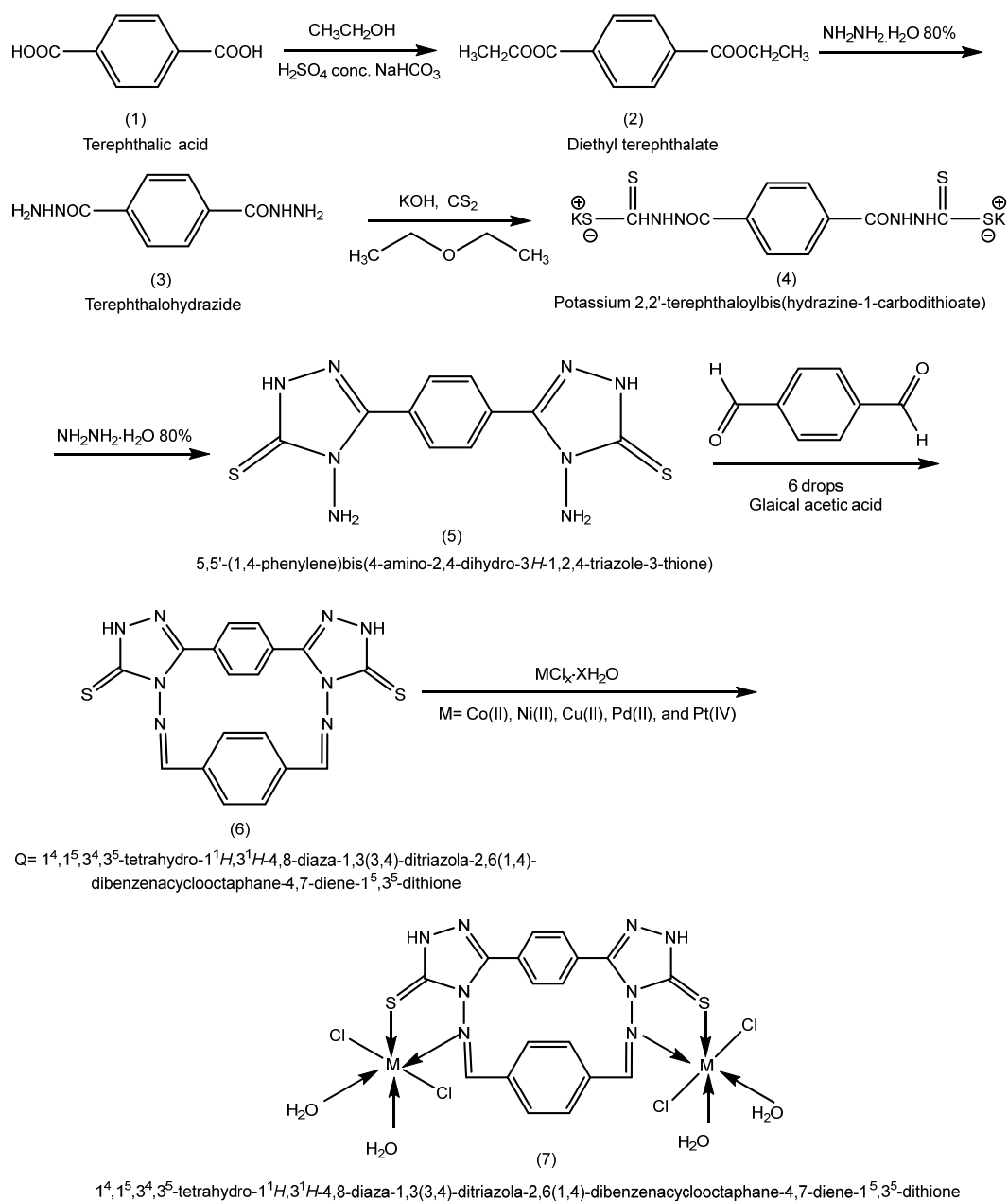
### Procedure

#### **Diethyl terephthalate synthesis – the initial step (2)**

According to the following scheme, diethyl terephthalate was synthesized [12]; 5 g of Terephthalic acid 0.03 mmol was dissolved in 45 mL of EtOH. The insertion of 5 mL of concentrated  $\text{H}_2\text{SO}_4$  rendered the reaction acidic. The reaction mixture was incubated under reflux for 6 h. To eliminate vacuum-filtered residual acid, the remaining alcohol is distilled- $\text{H}_2\text{O}$  and cooled with a 10% saturated sodium chloride followed by a sodium bicarbonate solution. Eventually, the diethyl terephthalate crystal was assembled.

#### **Terephthalohydrazide synthesis - the second step (3)**

The present route was used to synthesize the terephthalohydrazide [13] Scheme 1: Two point three grams of Diethyl terephthalate 0.01 mmol was immersed in 20 mL of ethanol. The mixture was then heated and refluxed for 10 h after appending 80% of the stated amount of hydrazine (35 mL). The reaction was assessed using thin-layer chromatography (TLC), and vacuum-dried and filtered solids were produced. Utilizing a white crystal needle and ice-cold water, the product was obtained in the form of a powder.



**Scheme 1.** The general synthetic route for new Schiff bases and their complexes

#### Potassium 2,2'-terephthaloyl bis-ester (hydrazine-1-carbodithioate) synthesis - the third step (4)

The present route follows Scheme 1 for the synthesis of potassium 2,2'-terephthaloylbis(hydrazine-1-carbodithioate). Ethanol was used to dissolve potassium-hydroxide (KOH) (35 mL). Terephthalohydrazide and carbon disulfide (CS<sub>2</sub>) were then inserted into the mixture, which was held at room temperature with stirring for 12 h. Diethyl ether (250 mL) had also been

inserted into the reaction and stirred for 10 min to cool down; diethyl ether was washed under vacuum after already being presented in a solid filter.

#### Synthesis of 5,5'-(1,4-phenylene)bis(4-amino-2,4-dihydro-3H-1,2,4-triazole-3-thione) - the fourth step (5)

The present route follows Scheme 1 to synthesize 5,5'-(1,4-phenylene)bis(4-amino-2,4-dihydro-3H-1,2,4-triazole-3-thione). Hydrazine hydrate 80% (35 mL) was

diluted with a compound (4) (0.0094 mmol). The blending has been overflowing for 6 h now. The greenish reaction abruptly changed color. In order to keep a perceive of the reaction, TLC was used. As an outcome, the tenor had already become acidic. Under vacuum, the precipitation was sprayed onto the compound.

#### **Synthesis of 1<sup>4</sup>,1<sup>5</sup>,3<sup>4</sup>,3<sup>5</sup>-tetrahydro-1<sup>1</sup>H,3<sup>1</sup>H-4,8-diaza-1,3(3,4)-diazola-2,6(1,4)-dibenzenacyclooctaphane-4,7-diene-1<sup>5</sup>,3<sup>5</sup>-dithione (Q) - the fifth step (6)**

Following Scheme 1, absolute ethanol was utilized to distribute and augment the concentration of compound (5) (0.0094 mmol) at a volume of 35 mL. Thereafter, terephthaldehyde was inserted (0.003 mmol). An acidic reaction was caused by the insertion of six drops of glacial acetic acid into the mixture. Under reflux, the mixtures were heated for approx. 10 h. To keep abreast of the reaction, TLC was used, and the eventual powder was filtered under vacuum.

#### **Synthesis of the transition metal complex - the sixth step (7)**

Transition metal complexes of Co(II), Cu(II), Ni(II), Pd(II), and Pt(IV) were synthesized from the metallic salts of CoCl<sub>2</sub>·6H<sub>2</sub>O, NiCl<sub>2</sub>·6H<sub>2</sub>O, CuCl<sub>2</sub>·2H<sub>2</sub>O, PdCl<sub>2</sub>·2H<sub>2</sub>O, and PtCl<sub>6</sub>·6H<sub>2</sub>O besides (Q), in 2:1 ratio of metal to ligand, following Scheme 1. It took 6 h of warming under reflux to finalize the reaction. The precipitate was filtered and eventually washed with distilled water.

#### **Films preparation technique of polyvinyl chloride**

The polymer polyvinyl chloride was dissolved by

tetrahydrofuran (THF) in a solution 0.5% w/v; after preparation, the solutions were poured into a glass frame, and small sinks with a capacity of 6 mL were created by attaching laboratory glass slides to a piece of ordinary glass to make this frame. As the solvent evaporated at 24 h, polymer films began to appear. These films have a thickness of around 40 μm, and are adhered to papers, with dimension holes of 2 × 2 cm.

## ■ RESULTS AND DISCUSSION

A new ligand from Schiff bases and their complexes are indicated by the information in Table 1, including experimental formula (C, H, N, and S), the ratio of metal to ligand, and the physical properties of the new ligand from Schiff base and their complexes. All complexes were soluble in DMSO-*d*<sub>6</sub>.

#### **The FTIR Spectra of the New Schiff Base (Q) and Their Complexes**

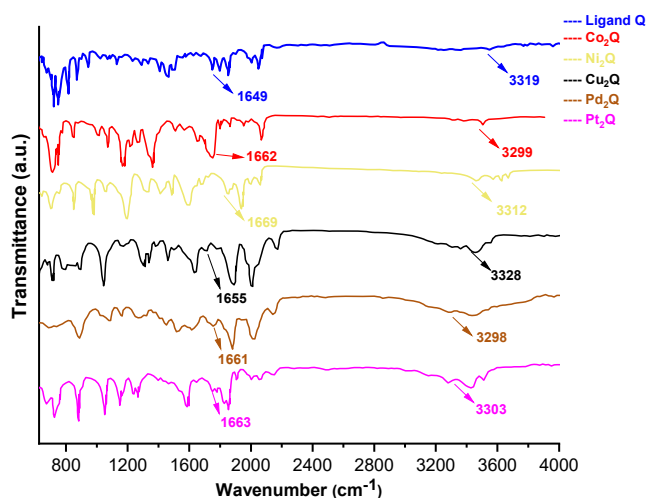
Diverse Schiff base ligands and their complexes were analyzed with FTIR spectrophotometry. Table 2 and Fig. 1 show the absorption variations for the ligand observed in the bands of N-H 3319 cm<sup>-1</sup> symmetry and asymmetry, CH=N 1649 cm<sup>-1</sup>, and C=S 1120 cm<sup>-1</sup>; the two groups of nitrogen and sulfur atoms observed the coordinate with a metal ion, although the complexes are revealed bands at 1662 cm<sup>-1</sup>, for CH=N [14], and 1117 cm<sup>-1</sup> for C=S, the ligand-Metal coordinate is responsible for shifting (Q) intensity. It is also conspicuous that there are new bands in the metals (Metal-N), (Metal-O),

**Table 1.** The physical properties and analytical data of the new Schiff base (Q) and its complexes

Comp.	Experimental formula	Color	M.P °C	Yield %	M.wt g.mol <sup>-1</sup>	Micro elemental analysis found (calc.)				Metal content % found (calc.)
						C%	H%	N%	S%	
Q	C <sub>18</sub> H <sub>12</sub> N <sub>8</sub> S <sub>2</sub>	Off-white	> 300	74	404.47	54.11 (53.45)	2.74 (2.99)	26.02 (27.70)	15.39 (15.85)	-
Co <sub>2</sub> Q	C <sub>18</sub> H <sub>24</sub> Co <sub>2</sub> Cl <sub>4</sub> N <sub>8</sub> S <sub>2</sub> O <sub>6</sub>	Yellowish	> 305	68	771.8	35.02 (35.51)	3.14 (4.59)	12.36 (12.66)	5.98 (7.78)	11.21 (10.08)
Ni <sub>2</sub> Q	C <sub>18</sub> H <sub>22</sub> Ni <sub>2</sub> Cl <sub>4</sub> N <sub>8</sub> S <sub>2</sub> O <sub>7</sub>	Dark Brown	285	71	785.4	27.37 (26.44)	2.99 (4.32)	12.94 (13.76)	6.43 (7.26)	10.41 (10.11)
Cu <sub>2</sub> Q	C <sub>18</sub> H <sub>20</sub> Cu <sub>2</sub> Cl <sub>4</sub> N <sub>8</sub> S <sub>2</sub> O <sub>4</sub>	Yellowish	> 310	66	745	28.37 (27.91)	2.67 (3.83)	13.88 (12.79)	6.21 (6.73)	15.29 (14.40)
Pd <sub>2</sub> Q	C <sub>20</sub> H <sub>26</sub> Pd <sub>2</sub> Cl <sub>4</sub> N <sub>8</sub> S <sub>2</sub> O	Light yellowish	> 315	73	812.8	26.93 (28.86)	1.86 (3.24)	12.33 (11.26)	6.29 (7.46)	21.43 (20.24)
Pt <sub>2</sub> Q	C <sub>18</sub> H <sub>24</sub> Pt <sub>2</sub> Cl <sub>8</sub> N <sub>8</sub> S <sub>2</sub> O <sub>2</sub>	Dark yellowish	294	68	1122	31.32 (30.11)	1.87 (2.65)	9.08 (9.51)	6.47 (6.13)	32.05 (33.00)

**Table 2.** FTIR spectrum data for new Schiff base (Q) and their metal complexes are observed

Symbol	FTIR ( $\nu$ , $\text{cm}^{-1}$ )						
	N-H	C=N	C=S	M-N	M-O	M-S	M-Cl
Q	3319	1649	1120	-	-	-	-
Co <sub>2</sub> Q	3299	1662	1117	607	554	441	398
Ni <sub>2</sub> Q	3312	1669	1109	612	542	448	390
Cu <sub>2</sub> Q	3328	1655	1084	601	539	499	391
Pd <sub>2</sub> Q	3298	1661	1099	598	547	472	388
Pt <sub>2</sub> Q	3303	1663	1097	591	566	489	362

**Fig 1.** FTIR spectrum for Schiff base (Q) and their metal ion complexes

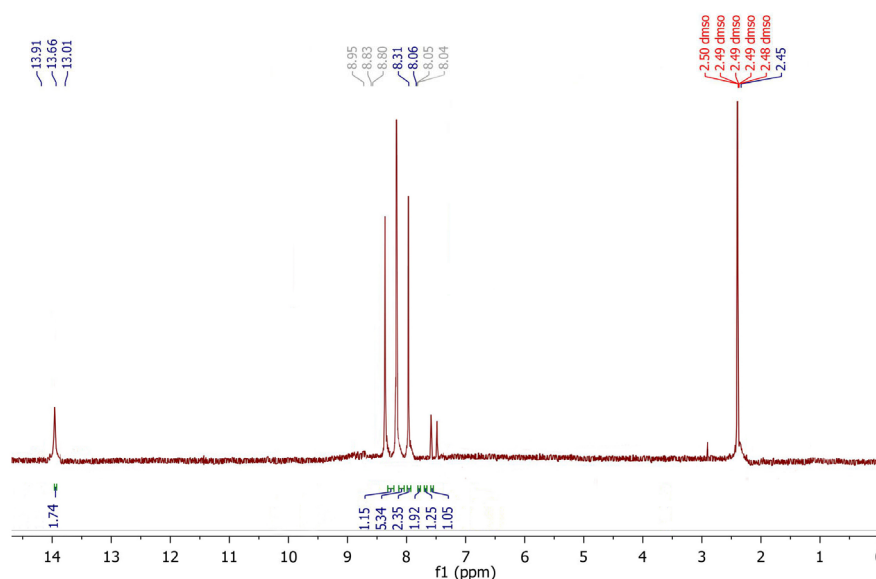
(Metal-S), and (Metal-Cl) in the range of 290–610  $\text{cm}^{-1}$ .

### NMR Spectra of Synthesized Compounds (Q)

Fig. 3 and Table 3 show the results of a <sup>13</sup>C-NMR spectrum of (Q) spotted the signals at  $\delta$ , ppm: 168 for CH=N (imine) [15], 161 for C=S thione group, 136 for C-C benzene ring; whereas in Fig. 2, and Table 3 showed the values of chemical shifts for the <sup>1</sup>H-NMR spectrum of (Q) spotted: 13.66 (1H, s, SH) thiol, 8.31 (4H, m, CH ar.) benzene ring, 7.93 (1H, m, CH=N) imine group.

### The Ultra-Violet Spectra of the New Schiff Bases (Q) and Their Complexes

Schiff bases were dissolved in chloroform and their complexes were derived from a variety of bands as a consequence; Fig. 4, and Table 4 show the ligand (Q) with three bands of absorption at 242 nm, 41322  $\text{cm}^{-1}$ , and 362 nm, 27624  $\text{cm}^{-1}$  allocated to  $\pi \rightarrow \pi^*$  and  $n \rightarrow \pi^*$

**Fig 2.** The <sup>1</sup>H-NMR spectrum of Schiff base (ligand Q)

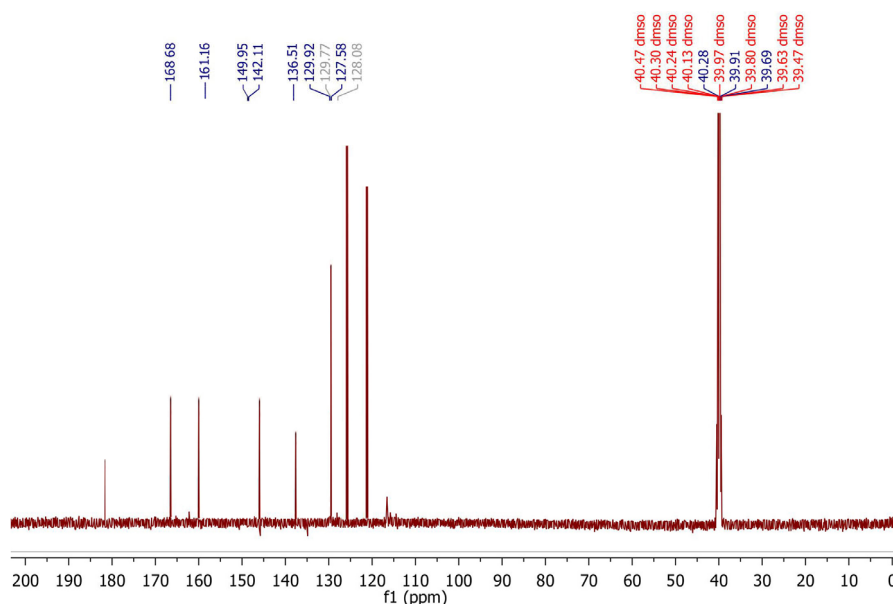


Fig 3.  $^{13}\text{C}$ -NMR spectrum of Schiff base (ligand Q)

Table 3. Data for the new Schiff base (Q) is shown in (NMR data)

Symbol	$^1\text{H}$ -NMR (500 MHz, $\text{DMSO}-d_6$ , $\delta$ , ppm in Hz)
Q	13.66 (1H, s, SH) thioI, 8.31 (4H, m, CH ar.), 7.93 (1H, m, CH=N) imine
Symbol	$^{13}\text{C}$ -NMR (125 MHz, $\text{DMSO}-d_6$ , $\delta$ , ppm in Hz)
Q	168 (CH=N) (imine), 161 (C=S) thione, 136 (C-C) benzene ring

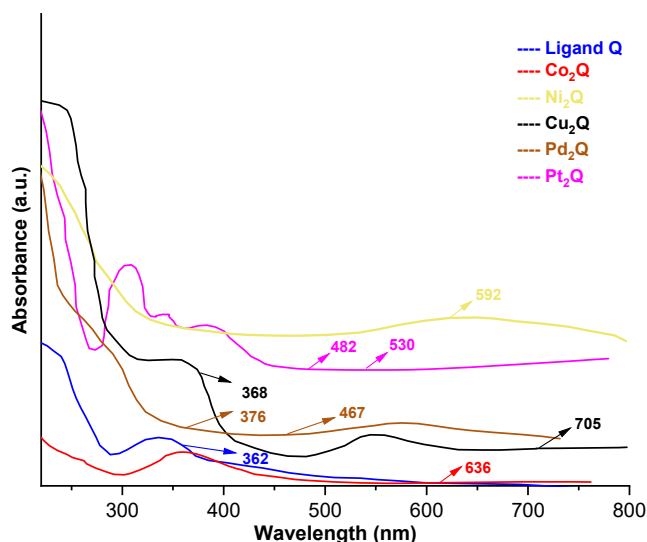


Fig 4. Electronic spectra of the ligand and their metal complexes

intra-ligand transition, and 421 nm,  $23752\text{ cm}^{-1}$  for  $n \rightarrow \pi^*$  whereas other complexes arranged to cobalt(II) complex two-bands at 636 nm,  $15723\text{ cm}^{-1}$  and 498 nm,  $20080\text{ cm}^{-1}$ ; nickel(II) complex two-bands at 592 nm,  $16891\text{ cm}^{-1}$  and

472 nm,  $21186\text{ cm}^{-1}$  for  $[^3\text{A}_2\text{g} \rightarrow ^3\text{T}_1\text{g}]$  (F)  $\nu_2$ , and  $[^3\text{A}_2\text{g} \rightarrow ^3\text{T}_1\text{g}]$  (P)  $\nu_3$ ; copper(II) complex  $[^2\text{E}_g \rightarrow ^2\text{T}_2\text{g}]$  [L  $\rightarrow$  Cu] (C.T.); palladium(II) complex were assigned to 467 nm,  $21413\text{ cm}^{-1}$ ; 376 nm,  $26595\text{ cm}^{-1}$ ; and 305 nm,  $32786\text{ cm}^{-1}$  for  $[^1\text{A}_1\text{g} \rightarrow ^1\text{B}_1\text{g}]$ ,  $[^1\text{A}_1\text{g} \rightarrow ^1\text{E}_1\text{g}]$  and [L  $\rightarrow$  Pd] (C.T.); platinum(IV) complex were assigned to 530 nm,  $18867\text{ cm}^{-1}$ ; 482 nm,  $20746\text{ cm}^{-1}$ ; and 433 nm,  $23094\text{ cm}^{-1}$   $[^1\text{A}_1\text{g} \rightarrow ^3\text{T}_1\text{g}]$ ,  $[^1\text{A}_1\text{g} \rightarrow ^3\text{T}_2\text{g}]$  and [L  $\rightarrow$  Pt] (C.T.).

### Thermal Analysis (TG) of the New Schiff Base (Q) and Its Complexes

Fig. 5 and Table 5 imply the Schiff base ligand (Q)'s thermogravimetric TG curve and their complexes under nitrogen gas ( $\text{N}_2$ ) in which temperatures ranged from 25 to 600  $^\circ\text{C}$  at a rate of 10  $^\circ\text{C}/\text{min}$ . In TGA, oven moisture is blended with gravimetric analysis, and there is a modest oven rod that records the temperature and weight of the specimen over time until that weight is somewhat constant. As a result of its high sensitivity to exothermic and endothermic processes and the ability to

**Table 4.** Molar conductivity and magnetic-susceptibility of metal-complexes

Compound	$\lambda_{\max}$ nm ( $\nu$ , $\text{cm}^{-1}$ )	Assignment	Molar conductivity $\text{Ohm}^{-1} \text{cm}^2 \text{mol}^{-1}$	Magnetic susceptibility (B.M.) (calc.) found	Suggested geometry
Ligand Q	242 (41322)	$(\pi \rightarrow \pi^*)$	-	-	Octahedral geometry
	362 (27624)	$(n \rightarrow \pi^*)$			
Co <sub>2</sub> Q	636 (15723)	$^4T_{1g} \rightarrow ^4A_{2g}$ (F)	10.65	(4.12) 4.22	Octahedral geometry
Ni <sub>2</sub> Q	592 (16891)	$^3A_{2g} \rightarrow ^3T_{1g}$ (F)	12.77	(2.75)	Octahedral geometry
	472 (21186)	$^3A_{2g} \rightarrow ^3T_{1g}$ (P)		2.79	
Cu <sub>2</sub> Q	705 368	$^2E_g \rightarrow ^2T_{2g}$ L $\rightarrow$ Cu C.T.	11.39	(1.73) 1.80	Octahedral geometry
	Pd <sub>2</sub> Q	467 (21413)		$^1A_{1g} \rightarrow ^1B_{1g}$	
Pt <sub>2</sub> Q		376 (26595)	$^1A_{1g} \rightarrow ^1E_{1g}$	19.04	0.02
	Pt <sub>2</sub> Q	530 (18867)	$^1A_{1g} \rightarrow ^3T_{1g}$		19.04
		482 (20746)	$^1A_{1g} \rightarrow ^3T_{2g}$	0.11	

**Table 5.** Thermal decomposition data for the new Schiff base ligand and its complexes

Comp.	Molecular formula M.wt.	Steps	Temp. range of the decomposition (TG) °C	The suggested formula for loss	Mass loss %	
					Cal.	Found
Q	C <sub>18</sub> H <sub>12</sub> N <sub>8</sub> S <sub>2</sub> 404.47	1	0–220	C <sub>6</sub> H <sub>4</sub> , 2S	34.61	32.87
		2	220–405	2N, 2C=N-NH	27.19	27.01
		3	405–595	2N, C <sub>6</sub> H <sub>4</sub>	25.71	24.66
Co <sub>2</sub> Q	C <sub>18</sub> H <sub>24</sub> Co <sub>2</sub> Cl <sub>4</sub> N <sub>8</sub> S <sub>2</sub> O <sub>6</sub> 771.8	1	0–190	2N, C <sub>6</sub> H <sub>4</sub> , 2H <sub>2</sub> O	18.13	18.02
		2	190–390	2C <sub>2</sub> N <sub>3</sub> H, C <sub>6</sub> H <sub>4</sub>	27.20	28.11
		3	390–595	4Cl, 4H <sub>2</sub> O	27.72	26.15
Ni <sub>2</sub> Q	C <sub>18</sub> H <sub>22</sub> Ni <sub>2</sub> Cl <sub>4</sub> N <sub>8</sub> S <sub>2</sub> O <sub>7</sub> 785.4	1	0–229	C <sub>6</sub> H <sub>4</sub> , H <sub>2</sub> O	11.96	10.09
		2	229–377	2N, 2S, 2C <sub>2</sub> N <sub>3</sub> H	28.77	27.38
		3	377–595	C <sub>6</sub> H <sub>4</sub> , 4Cl, 3H <sub>2</sub> O	34.63	34.06
Cu <sub>2</sub> Q	C <sub>18</sub> H <sub>20</sub> Cu <sub>2</sub> Cl <sub>4</sub> N <sub>8</sub> S <sub>2</sub> O <sub>4</sub> 745	1	0–268	2C <sub>2</sub> N <sub>3</sub> H, C <sub>6</sub> H <sub>4</sub>	28.18	28.66
		2	268–405	C <sub>6</sub> H <sub>4</sub> , 2S, 2N	22.55	20.82
		3	405–595	4H <sub>2</sub> O, 3Cl	23.95	21.87
Pd <sub>2</sub> Q	C <sub>20</sub> H <sub>26</sub> Pd <sub>2</sub> Cl <sub>4</sub> N <sub>8</sub> S <sub>2</sub> O 812.8	1	0–228	CH <sub>3</sub> CH <sub>2</sub> OH	5.65	6.02
		2	228–395	2S, 2N, 2C <sub>2</sub> N <sub>3</sub> H	27.80	26.24
		3	395–595	2C <sub>6</sub> H <sub>4</sub> , 2Cl, 4H <sub>2</sub> O	36.29	34.98
Pt <sub>2</sub> Q	C <sub>18</sub> H <sub>24</sub> Pt <sub>2</sub> Cl <sub>8</sub> N <sub>8</sub> S <sub>2</sub> O <sub>2</sub> 1122	1	0–270	2H <sub>2</sub> O, C <sub>6</sub> H <sub>4</sub>	9.98	10.20
		2	270–350	2N-NH, 4N, 2S	15.86	14.54
		3	440–595	C <sub>6</sub> H <sub>4</sub> , 4Cl, 3H <sub>2</sub> O	24.24	23.66

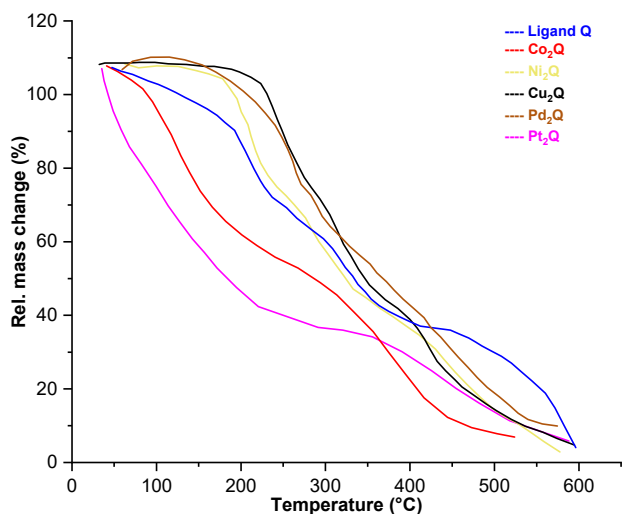


**Fig 5.** Thermogravimetric (TG) curve of ligands and their complexes by heating 10 °C/min under nitrogen gas

evaluate temperature-dependent variations in physical and chemical properties, heat capacity can be judged. Most weight losses happened during the later disintegration, and the final deterioration resulted in a weight loss of more than 60% overall. As a result, the thermal vaporization of volatile substances was revealed as the first stage in the decomposition of complexes after moisture evaporation. Depleting molecules from the complexes presumably caused the second stage of deterioration. The Schiff base ligand Q also shows two stages of decomposition and subsequent dehydration. The DTG curves similarly exhibited a slight peak affiliated with moisture loss, a steep summit with maximum temperature values as shown in Table 5 as well as a slight decrease associated with moisture loss, except for Pt<sub>2</sub>Q, which had a large, broad peak between 600 and 800 °C. The break-down temperatures of all the combinations were virtually the same, ranging from 150 to 330 °C, proving their thermal stability. To validate the complexes' relative stability, the temperature at which deterioration began has been proposed. In contrast to the Pt<sub>2</sub>Q complex, degradation persisted at temperatures above 800 °C.

### Photostability

The photostability of the Schiff base and five metal complexes of Co(II), Ni(II), Cu(II), Pd(II), and Pt(IV) modified with polyvinyl chloride films was performed by

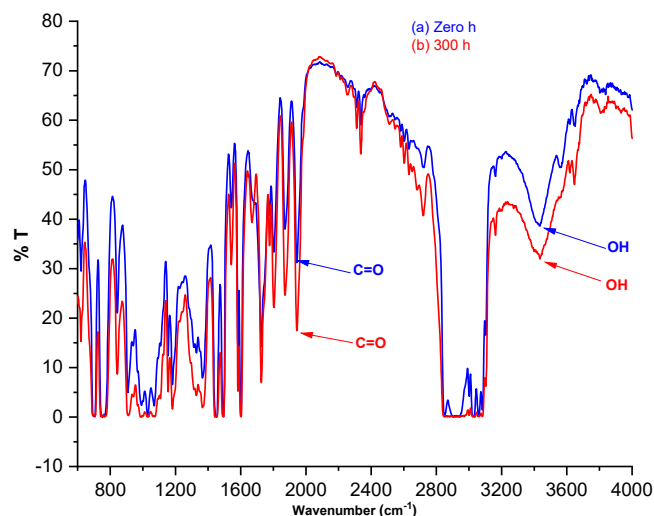


**Fig 6.** The FTIR spectra of a PVC film (a) before and (b) after 300 h of exposure

dissolving in tetrahydrofuran (THF) at 25 °C. It can be seen in the 3600–3200 cm<sup>-1</sup> band where a large-band occurs that weakens the band's strength in the FTIR spectrum; this is responsible for the formation of hydroxyl, carbonyl, and polyene groups [16] as shown in Fig. 6. I<sub>OH</sub>, I<sub>CO</sub>, I<sub>PO</sub> indices are shown in Fig. 7–9 where the raying sensitivity period was comparative to PVC without addition and raises the exposure ray rate of I<sub>OH</sub>, I<sub>CO</sub>, and I<sub>PO</sub>.

Fig. 7–9 show a significant rise in exposure ray rate of I<sub>OH</sub>, I<sub>CO</sub>, and I<sub>PO</sub> indices compared to PVC films without the additament of sensitivity raying time, with the addition of metals such as copper, nickel and platinum(IV) which was inferred to be the majority effective photo-stabilizer.

### PVC Films Molecular Average Weight Changes as an Outcome of Photolysis

A significant chain collapse at a distant place in the PVC chain caused a rapid decline in  $\overline{M}_v$  in Fig. 11, revealing that PVC degradation attributed to the reduced scale of PVC in Fig. 10. The  $\overline{M}_v$  versus exposure plot proves that the film was irradiated an extra 0.5% of the time. S is the actual population of chain scissors in Fig. 12, (Eq. (1)) [17].

$\overline{M}_v,0$  = M.wt viscosity means at the foremost of the experiment;

$\overline{M}_v, t$  = M.wt viscosity on average during irradiation

$$S = \frac{\overline{Mv,0}}{\overline{Mv,t}} - 1 \quad (1)$$

Since cross-linking can determine the level of retrogradation premised on branching in Fig. 13, it thus indicates a rise in data. ( $\alpha$ ) via Eq. (2) are:

$m$  = Primitive of M.wt

$$\alpha = \frac{m \times S}{\overline{Mv}} \quad (2)$$

The degree of retrograde rate ( $\alpha$ ) versus the time of radiation as shown in Fig. 14, the primary phases of PVC, grade assembly (D.P.) and the number of PVC monomeric unit (Eq. (3)) illustrates the degree of irradiation; Reverse polymerizing ( $1/DP_n$ ) versus an inverted sample in front of a blank demonstrates an augmentation in radiation time ( $1/DP_n$ ).

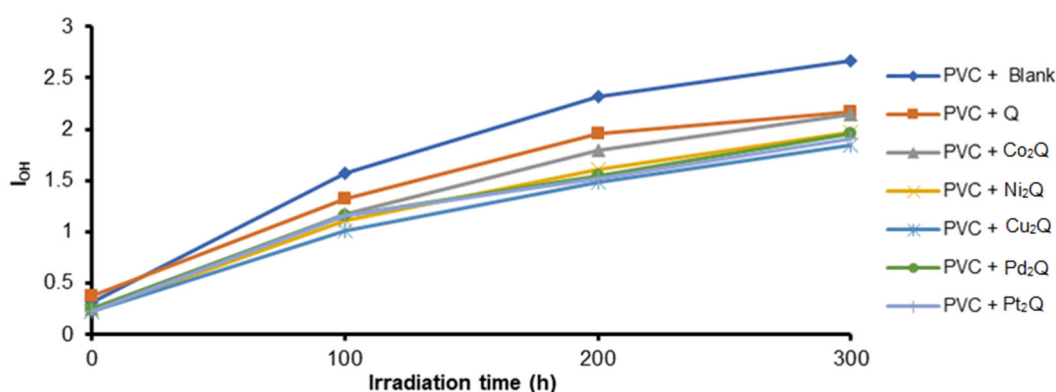


Fig 7. The relationship between ( $I_{OH}$ ) and irradiation time for PVC films ( $40 \mu\text{m}$ ) containing 0.5% additives

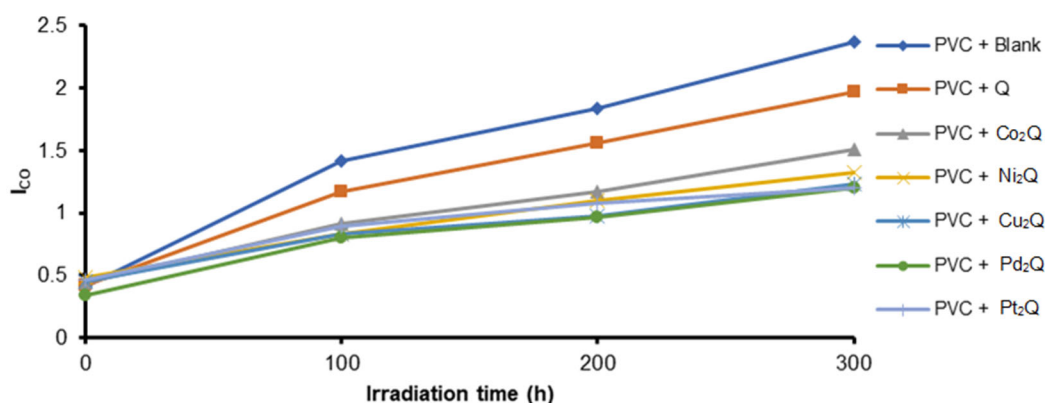


Fig 8. The relationship between ( $I_{CO}$ ) and irradiation time for PVC films ( $40 \mu\text{m}$ ) containing 0.5% additives

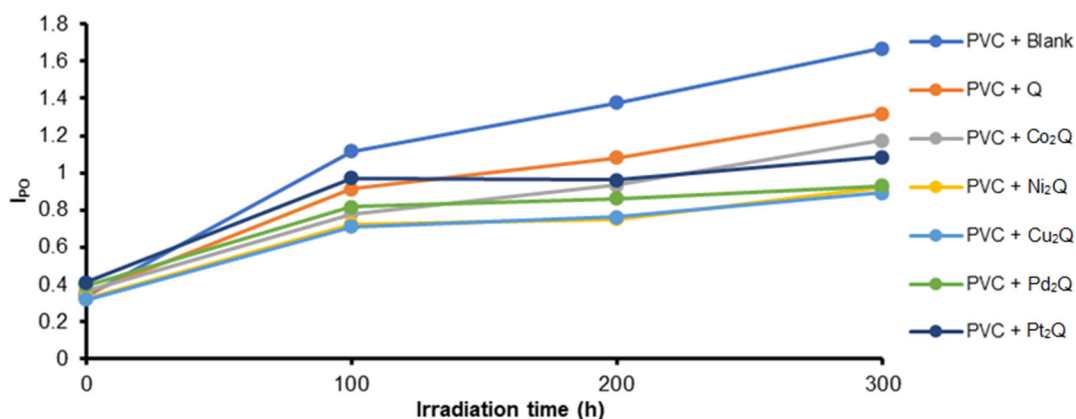


Fig 9. The relationship between ( $I_{PO}$ ) and irradiation time for PVC films ( $40 \mu\text{m}$ ) containing 0.5% additives

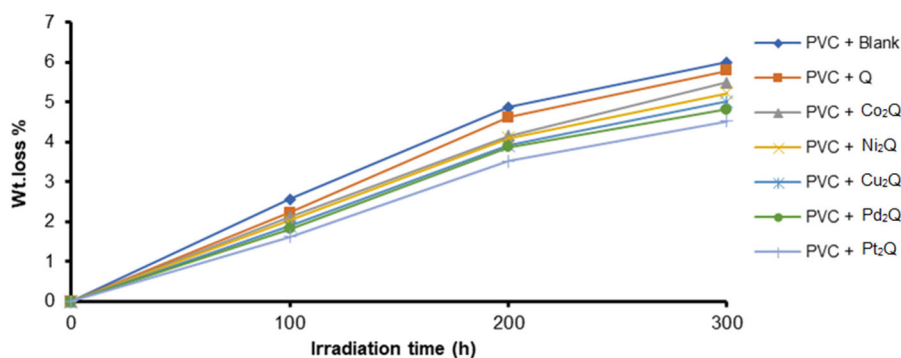


Fig 10. Variation of the weight loss of PVC films (40  $\mu\text{m}$ ) thickness containing 0.5% additives with the irradiation time

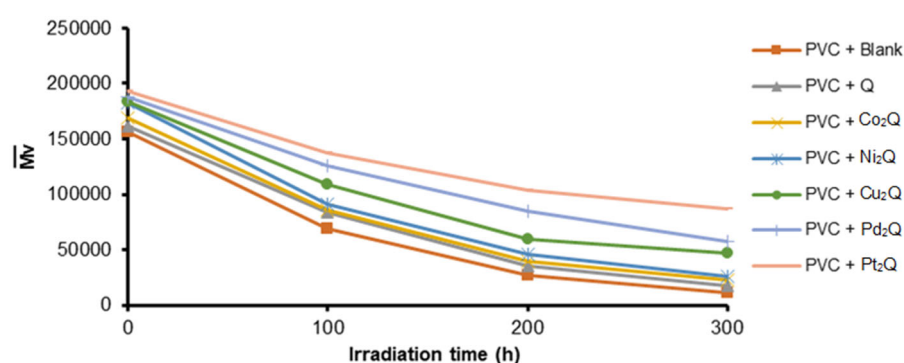


Fig 11. Variation of the M.wt. average for PVC films (40  $\mu\text{m}$ ) thickness containing 0.5% additives with the irradiation time

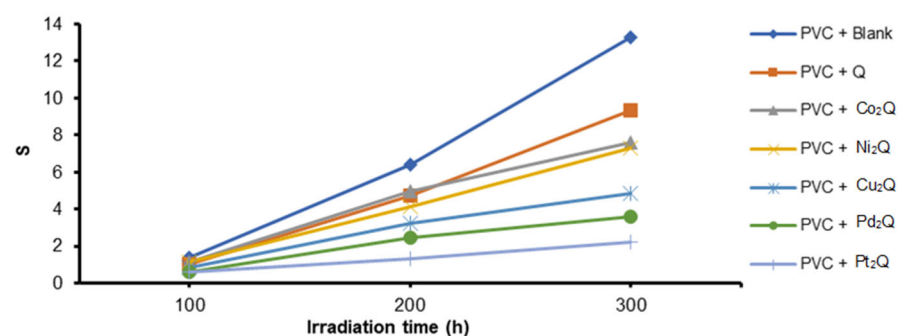


Fig 12. Variation of the Increase growth in the degree of branching (S) for PVC films (40  $\mu\text{m}$ ) thickness containing 0.5% additives with the irradiation time

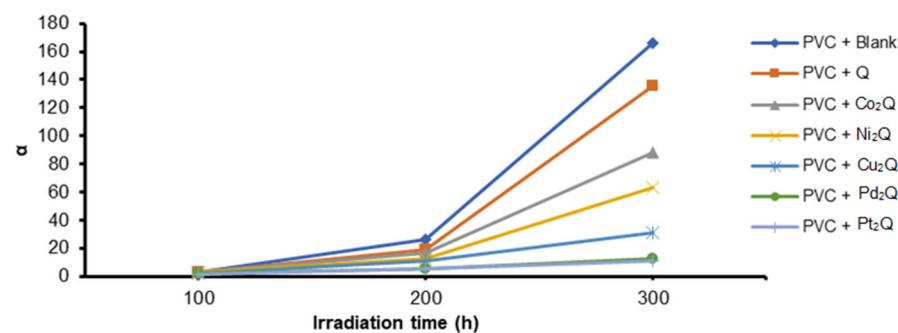
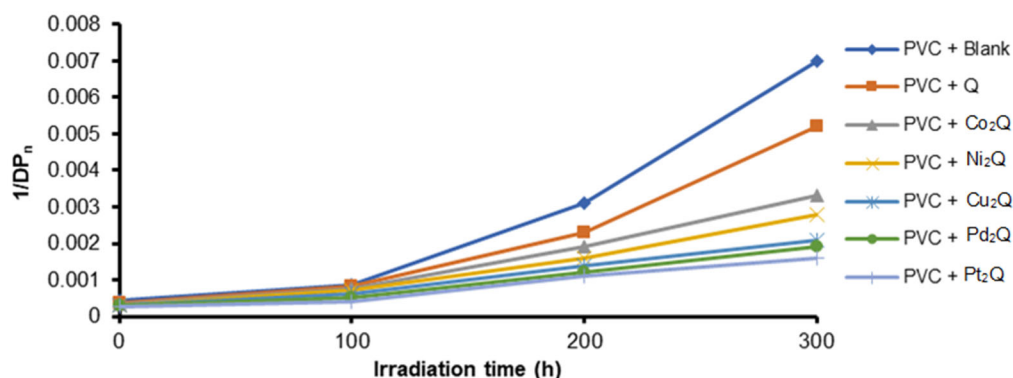


Fig 13. Variation of degree of degradation ( $\alpha$ ) for PVC films (40  $\mu\text{m}$ ) thickness containing 0.5% additives with the irradiation time



**Fig 14.** Variation of degree of polymerization ( $1/DP_n$ ) for PVC films ( $40 \mu\text{m}$ ) thickness containing 0.5% additives with the irradiation time

$M_n$  = the molecular weight M.wt. average number

$$DP_n = X_n = \frac{M_n}{M_o} \quad (3)$$

It is calculated that the first-order-rate constant ( $K_d$ ) [18] of all modified polymer films in these additive polymers are UV-light stable because photo-stabilizers [19] always have low  $K_d$  values. Photo-stabilizers, the category of additives in PVC films, have an influence on  $K_d$  values, which reduces in the order specified in Table 6.

The investigated photo-stabilizers stabilizing effectiveness was demonstrated to go in the following sequence:



### Proposed Stabilization Mechanisms for PVC Additives

The 1,2,4-triazole-3-thione ring is crucial in photo-stabilization if ultra-violet (UV) light absorption results from radical scavenging and peroxide degeneration, absorption exposures cause the aromatic ring's UV energy to decrease [20] in PVC photography stability. There is a possibility that the complex of chromophores [21] will develop radical cavities due to the transmission energy amongst chelates and chromophore excitations being sustained. All this work on film stabilization use the resonance resonant suggested in Scheme 2. Polymer (C-C) bonds are degraded when exposed to UV light over an extended period. Because of the effects of photostabilization and photo degradation [22], the following procedure might lead to energy transmission in

**Table 6.** Photodecomposition rate constants ( $K_d$ ) irradiation time for PVC films ( $40 \mu\text{m}$ ) containing 0.5% additives

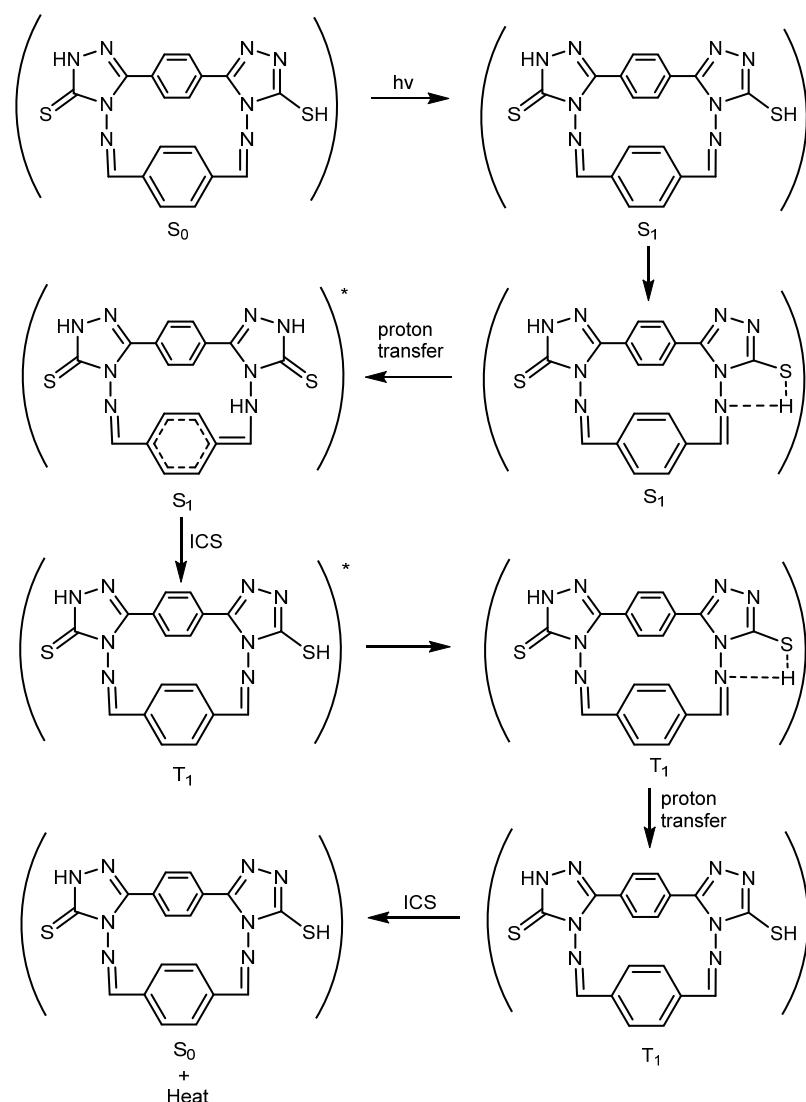
Compound	$K_d$ ( $S^{-1}$ )
PVC + Blank	$6.221 \times 10^{-3}$
PVC + Q	$5.361 \times 10^{-3}$
PVC + Co <sub>2</sub> Q	$3.319 \times 10^{-3}$
PVC + Ni <sub>2</sub> Q	$3.118 \times 10^{-3}$
PVC + Cu <sub>2</sub> Q	$2.729 \times 10^{-3}$
PVC + Pd <sub>2</sub> Q	$1.995 \times 10^{-3}$
PVC + Pt <sub>2</sub> Q	$1.257 \times 10^{-3}$

polymers that is highly ineffective. The energy is transferred between molecules of a photo-stabilizer (acceptor) [23] and a stimulating polymer molecule (donor) [24]. Intra molecular [23] energy exchange happens between the molecules of a polymer (acceptor) and another chromophore (donor).

### Surface Morphology for PVC Photodegradation Evaluation

Individual polymer chains are visualized in their configuration and in some cases, single atoms can be observed. Although microscopic [25] techniques are widely used in the study of polymers and are very popular, little is known about their applications to the study of polymer degradation processes.

In UV-irradiated specimens, chain scission, branching and cross-linking [26], polyene fashioning, oxidation hydroxyl and hydroperoxide groups, and rearrangement processes are the main reactions. The



**Scheme 2.** The suggested mechanism of photostabilization of PVC by Q ligand through absorption of UV light and dissipation of light energy as heat

specimen surface is where oxidation reactions are primarily localized and are influenced by its morphology [27]. As a result of their sensitivity to light and the elevation activity of the intermediate free-radical [28] fashioning, photodegradation products can speed-up the further destruction of specimens. Exposure to specimens typically causes the specimens to become brittle and yellow, and the films to shrink. It was discovered that the deterioration and evolution of volatile products led to the fashioning of cracks and holes.

Microscopy visuals of PVC films exposed to 300 h of UV-lamp in the air are shown in Fig. 15 in order to begin

polymer decomposition, active free radicals can eliminate hydrogen atoms from macromolecules [29]; crack development was observed to increase with irradiation time in PVC films devoid of any additives; film embrittlement raises as photodegradation occurs in the presence of UV light; lighter cracks can be seen in PVC samples photodegraded with the additament of Cu(II) and Pt(IV) complexes. The chain scission reaction in photodegraded samples is directly linked to the formation of micro-cracks [30] on the polymer surface. It takes up more space than the original macromolecules when polymer bonds are damaged, resulting

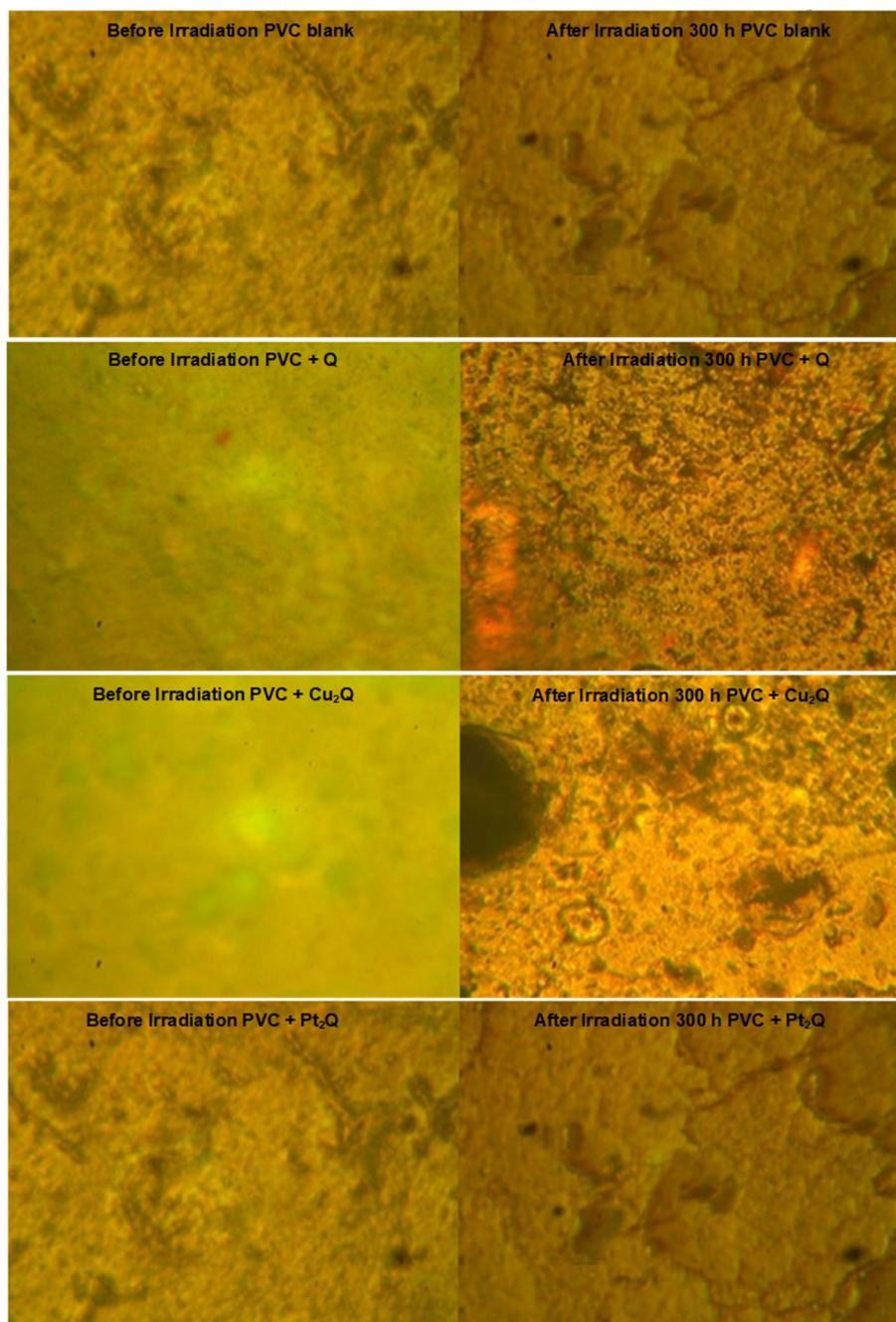


**Fig 15.** Surface morphologies (460× magnification) before and after 300 h of irradiation, microscopic images of PVC films (40 μm) blank and their complexes films were achieved

in more fragments. UV irradiated polymer film can be damaged by micro-cracks forming as a result of the strains and stresses [31] induced by this break-down of internal defects such as cracks or impurities that are frequently responsible for the formation of cracks; undegraded PVC film does not have a unique micro-structure; the films are smooth and without any visible structural flaws.

UV radiation of polymers often leave behind micro pores of varying shapes and sizes as the volatile [32] vapor degradation products exit; holes were shown in a photodegraded PVC film as an example, due to hydrogen abstraction and the main chain scission reaction [31] PVC's chemical structure is very simple, consisting of varying ethylene and chloride groups, due

to the voids and holes formed, the number of adsorbent surface and diffusion channels increases for the volatile, low molecular product, mainly HCl. As an outcome oxygen rapidly diffuses into the packing of the polymer, resulting in even more rapid oxidation of PVC films.

## ■ CONCLUSION

The Schiff bases ligand (Q) were synthesized by using a 2-amino-triazole derivative and 4-phenoxybenzaldehyde by using the procedure reported in the literature. The novel ligand (Q) evinced bi-dentate behaviour in all metal complexes namely cobalt(II), nickel(II), copper(II), palladium(II), and platinum(IV) metal ions that coordinate with thiol group and nitrogen of dimethyldiazene. The ratio between complexes and new ligand relying on 2:1 molar ratio; The identification of the ligand and their complexes utilize several spectroscopic analysis namely FTIR, <sup>1</sup>H-NMR, <sup>13</sup>C-NMR and other techniques such as flame atomic absorption, magnetic susceptibility measurements, thermal analysis, C, H, N, and S elemental analyses and molar conductance. The outcomes revealed the the suggested complexes' structures that had an octahedral shape, except for palladium that had a tetrahedral geometry. The sequence of these complexes and ligands for photostabilization effectiveness is Pt<sub>2</sub>Q > Pd<sub>2</sub>Q > Cu<sub>2</sub>Q > Ni<sub>2</sub>Q > Co<sub>2</sub>Q > Q > PVC blank. Fig. 10. showed that the rate of molecular weight reduction, weight loss, hydroxyl, carbonyl, and polyene groups was excellent and showed slight variation over time. The complex containing Pt-complex was more effective as a photo-stabilizer.

## ■ ACKNOWLEDGMENTS

We thank Baghdad and Mustansiriyah Universities for technical support.

## ■ AUTHOR CONTRIBUTIONS

Ali Mudher Abdulkareem Al-Khazraji conceived and designed the experiments, conducted the experiments, analyzed the data, wrote the paper, provided funds, and revised the paper. The author also discussed the findings and improved the final text of the paper.

## ■ REFERENCES

- [1] Numan, A.T., 2010, Synthesis and spectral studies for new Schiff base and its binuclear complexes with Zn<sup>II</sup>, Cd<sup>II</sup> and Hg<sup>II</sup>, *Ibn Al-Haitham J. Pure Appl. Sci.*, 23 (2), 65–75.
- [2] Sellami, M., Bragazzi N.L., Slimani M., Hayes L., Jabbour G., De Giorgio A., and Dugué, B., 2019, The effect of exercise on glucoregulatory hormones: A countermeasure to human aging: Insights from a comprehensive review of the literature, *Int. J. Environ. Res. Public Health*, 16 (10), 1709.
- [3] Yang, L., Bajinka, O., Jarju, P.O., Tan, Y., Taal, A.M., and Ozdemir, G., 2021, The varying effects of antibiotics on gut microbiota, *AMB Express*, 11 (1), 116.
- [4] Maoka, T., 2020, Carotenoids as natural functional pigments, *J. Nat. Med.*, 74 (1), 1–16.
- [5] Dixit, D., Verma, P.K., and Marwaha, R.K., 2021, A review on 'triazoles': Their chemistry, synthesis and pharmacological potentials, *J. Iran. Chem. Soc.*, 18 (10), 2535–2565.
- [6] Al-Khazraji, A.M.A., and Al Hassani, R.A.M., 2020, Synthesis, characterization and spectroscopic study of new metal complexes form heterocyclic compounds for photostability study, *Syst. Rev. Pharm.*, 11 (5), 535–555.
- [7] Al-Khazraji, A.M.A., Al Hassani, R.A.M., and Ahmed, A., 2020, Studies on the photostability of polystyrene films with new metals complex of 1,2,4-triazole-3-thione derivate, *Sys Rev Pharm.*, 11 (5), 525–534.
- [8] Cordes, E.H., and Jencks, W.P., 1962, On the mechanism of Schiff base formation and hydrolysis, *J. Am. Chem. Soc.*, 84 (5), 832–837.
- [9] Endo, K., 2002, Synthesis and structure of poly(vinyl chloride), *Prog. Polym. Sci.*, 27 (10), 2021–2054.
- [10] Saad, H.A.R., Shakir, R.M., and Mahdi, M.H., 2018, Synthesis and thermal electro conductivity of some new triazole derivatives bearing azo or azomethain group, *Ibn Al-Haitham J. Pure Appl. Sci.*, 31 (3), 88–101.

- [11] Kryczyk-Poprawa, A., Kwiecień, A., and Opoka, W., 2019, Photostability of topical agents applied to the skin: A review, *Pharmaceutics*, 12 (1), 10.
- [12] Panwar, H., and Singh S., 2011, Synthesis and characterization of 3-aryl-5H,13aH-quinolino(3,2-f)(1,2,4)triazolo(4,3-b)(1,2-diaza-4-sulpho)azepines: *In vitro* antifungal and antibacterial activity, *Indones. J. Chem.*, 11 (2), 148–153.
- [13] Al-Mohammadi, N.A.H.A.H., Al-Fahdawi, A.S.M., and Al-Janabi, S.S.I., 2021, Design and characterization of new dinuclear macrocyclic dithiocarbamate complexes by the preparation of a free ligand derived from isopropylamine, *Iraqi J. Sci.*, 62 (1), 1–15.
- [14] Shekhawat, A., Singh, N., and Chundawat, N., 2022, Synthesis, characterization and biological activities of Schiff's base metal complexes derived from hydroxy trizene and aromatic aldehyde, *J. Sci. Res.*, 14 (1), 387–394.
- [15] Prakash, V., 2017, Applications of vanillin Schiff base ligands and their complexes: A review, *Int. J. Eng. Res. Sci.*, 3 (2), 36–47.
- [16] Chen, C., Chen, L., Yao, Y., Artigas, F., Huang, Q., and Zhang, W., 2019, Organotin release from polyvinyl chloride microplastics and concurrent photodegradation in water: Impacts from salinity, dissolved organic matter, and light exposure, *Environ. Sci. Technol.*, 53 (18), 10741–10752.
- [17] Cross, M.M., 1969, Polymer rheology: Influence of molecular weight and polydispersity, *J. Appl. Polym. Sci.*, 13 (4), 765–774.
- [18] Seo, H.J., Lee, J.W., Na, Y.H., and Boo, J.H., 2020, Enhancement of photocatalytic activities with nanosized polystyrene spheres patterned titanium dioxide films for water purification, *Catalysts*, 10 (8), 886.
- [19] Watheq, B., Yousif, E., Al-Mashhadani, M.H., Mohammed, A., Ahmed, D.S., Kadhom, M., and Jawad, A.H., 2020, A surface morphological study, poly(vinyl chloride) photo-stabilizers utilizing ibuprofen tin complexes against ultraviolet radiation, *Surfaces*, 3 (4), 579–593.
- [20] Ankamah, E., Sebag, J., Ng, E., and Nolan, J.M., 2019, Vitreous antioxidants, degeneration, and vitreo-retinopathy: Exploring the links, *Antioxidants*, 9 (1), 7.
- [21] Chamas, A., Moon, H., Zheng, J., Qiu, Y., Tabassum, T., Jang, J.H., Abu-Omar, M., Scott, S.L., and Suh, S., 2020, Degradation rates of plastics in the environment, *ACS Sustainable Chem. Eng.*, 8 (9), 3494–3511.
- [22] Yousif, E., Ahmed, D.S., Ahmed, A.A., Hameed, A.S., Muhamed, S.H., Yusop, R.M., Redwan, A., and Mohammed, S.A., 2019, The effect of high UV radiation exposure environment on the novel PVC polymers, *Environ. Sci. Pollut. Res.*, 26 (10), 9945–9954.
- [23] Minsker, K.S., Kolesov, S.V., Kulish E.I., Zaikov, G.E., 2019, "PVC Degradation in Blends with Other Polymers" in *Polymer Yearbook 13*, Eds. Pethrick, R.A., Zaikov, G., Tsuruta, T., and Koide, N., CRC Press, Boca Raton, Florida, 5–20.
- [24] Mohamed, N.A., and Al-Harby, N.F., 2021, Enhancement of the thermal stability of PVC filled with multiwalled carbon nanotubes using new antimicrobial itaconimido aryl 1,3,4-oxadiazoles, *Polym. Compos.*, 42 (3), 1245–1257.
- [25] Hendrickson, E., Minor, E.C., and Schreiner, K., 2018, Microplastic abundance and composition in western Lake Superior as determined via microscopy, Pyr-GC/MS, and FTIR, *Environ. Sci. Technol.*, 52 (4), 1787–1796.
- [26] Ainali, N.M., Bikiaris, D.N., and Lambropoulou, D.A., 2021, Aging effects on low-and high-density polyethylene, polypropylene and polystyrene under UV irradiation: An insight into decomposition mechanism by Py-GC/MS for microplastic analysis, *J. Anal. Appl. Pyrolysis*, 158, 105207.
- [27] Zhao, T., Cao, C., Wang, H., Shen, X., Lai, H., Zhu, Y., Chen, H., Han, L., Rehman, T., and He, F., 2021, Highly efficient all-polymer solar cells from a dithieno[3,2-f:2',3'-h] quinoxaline-based wide band gap donor, *Macromolecules*, 54 (24), 11468–11477.
- [28] Gao, Y., Zhou, D., Lyu, J., A, S., Xu, Q., Newland,

- B., Matyjaszewski, K., Tai, H., and Wang, W., 2020, Complex polymer architectures through free-radical polymerization of multivinyl monomers, *Nat. Rev. Chem.*, 4 (4), 194–212.
- [29] Jia, P., Hu, L., Shang, Q., Wang, R., Zhang, M., and Zhou, Y., 2017, Self-plasticization of PVC materials via chemical modification of mannich base of cardanol butyl ether, *ACS Sustainable Chem. Eng.*, 5 (8), 6665–6673.
- [30] Al-Salem, S.M., Behbehani, M.H., Al-Hazza'a, A., Arnold, J.C., Alston, S.M., Al-Rowaih A.A., Asiri, F., Al-Rowaih, S.F., and Karam, H., 2019, Study of the degradation profile for virgin linear low-density polyethylene (LLDPE) and polyolefin (PO) plastic waste blends, *J. Mater. Cycles Waste Manage.*, 21 (5), 1106–1122.
- [31] Vijayan, K., Muniyandi, M., and Munusamy, Y., 2021, Impact modified polyvinyl chloride based thermoplastic elastomers: effect of nitrile butadiene rubber and graphene oxide loading, *J. Eng. Sci.*, 17 (1), 51–74.
- [32] Apel, P.Y., 2019, Fabrication of functional micro- and nanoporous materials from polymers modified by swift heavy ions, *Radiat. Phys. Chem.*, 159, 25–34.